J. Electrochem. Sci. Eng. **16** (2026) 2919; http://dx.doi.org/10.5599/jese.2919

Open Access : ISSN 1847-9286
https://pub.iapchem.org/ojs/index.php/JESE

Original scientific paper

Fabrication of iridium-gold nanocomposite for the detection of selective serotonin reuptake inhibitors

Simone Barry[1,✉], Candice Cupido[1], Keagan Pokpas[1], Takalani Mulaudzi[2] and Rachel Fanelwa Ngece-Ajayi[1,✉]

[1]*SensorLab, Chemistry Department, Chemical Sciences Building, Senate Avenue, University of the Western Cape, Robert Sobukwe Road, Cape Town 7530, South Africa*

[2]*Molecular Sciences and Biochemistry Laboratory, Biotechnology Department, Life Sciences Building, Senate Avenue, University of the Western Cape, Robert Sobukwe Road, Cape Town 7530, South Africa*

Corresponding authors: ✉*2917596@myuwc.ac.za*; ✉*fngece@uwc.ac.za*; Tel.: +2721959-3049; Fax.: +2721959-3055

Received: July 30, 2025; Accepted: October 11, 2025; Published: October 18, 2025

Abstract

A comprehensive study of the development of a novel electrochemical sensor based on iridium-gold nanocomposite (IrAuNPs) modified electrodes for the detection of antidepressants, paroxetine (PRX) and citalopram (CIT) was conducted. The sensing platform, based on a glassy carbon electrode, was modified by drop-casting IrAuNPs, which allowed for enhanced conductivity. IrAuNPs, along with their counterparts iridium nanoparticles (IrNPs) and gold nanoparticles (AuNPs), were synthesized from coffee waste extract (CWE) via complete green chemistry. The physicochemical properties of synthesized nanomaterials were characterized using ultraviolet-visible spectroscopy, dynamic light scattering, high-resolution transmission electron microscopy, Fourier-transform infrared spectroscopy, cyclic voltammetry and square wave voltammetry. Results showed that the CWE could reduce the respective metallic salts to form mostly near-spherical to spherical IrAuNPs, IrNPs and AuNPs with core sizes ranging from 2.02 nm to 13.27 nm. The electrochemical sensor could determine PRX and CIT in the concentration ranges of 20 to 200 nM and 1 to 10 µM, with detection limits of 0.072 nM and 0.085 µM, respectively. The sensor showed a recovery of 86 to 115.1 %. The proposed sensor demonstrated good precision and accuracy, with excellent sensitivity and selectivity for drug identification in a rapid analysis time, which is crucial for applications in biological matrices.

Keywords

Coffee (*Coffea arabica L.*) waste; green nanotechnology; bimetallic nanoparticles; citalopram; paroxetine; electrochemical sensor

Introduction

Depression is a common and widespread mental disorder affecting ~350 million people worldwide [1]. It has become the leading cause of disability and has been listed as the third largest cause of disease burden since 2008 and is expected to rank first by 2030 [2]. Selective serotonin reuptake inhibitors (SSRIs) are one of the most prescribed classes of antidepressants [3]. Paroxetine (PRX) (3S,4R)-3-[(1,3-benzodioxol-5-yloxy) methyl]-4-(4-fluorophenyl) piperidine [4] and citalopram (CIT) (1-[3-(dimethylamino) propyl-]-1-(4-fluorophenyl)-1,3 dihydroisobenzo furan-5 carbonitrile) are potent SSRIs [5] commonly prescribed for the treatment of patients suffering from depression and for the management of generalized panic and anxiety disorders, obsessive-compulsive disorders [6], post-traumatic stress, and social phobia [7]. These SSRIs have also been recommended for treating body dysmorphia, premenstrual dysphoric disorder, presumed serotonergic component [8] and Huntington as well as multiple pain conditions [9].

These SSRIs act by selectively inhibiting the presynaptic recovery of serotonin at the serotonin transporter, causing an increase in serotonin at the postsynaptic membrane in the serotonergic synapse, thus improving depressive symptoms and the cognitive function of patients [10].

Antidepressant drug therapy has shown a high variability in the individual's response, ranging from severe adverse effects to failure or delayed therapeutic responses [11]. Paroxetine is the least well-tolerated SSRI and is associated with high rates of treatment discontinuation [12]. Citalopram is among the most frequently prescribed antidepressants in paediatric patients, yet 50 % of these patients fail to respond [13]. A few side effects of these SSRIs consumption are known as vision changes, weakness, drowsiness, dizziness, sweating, anxiety, sleep problems (insomnia), loss of appetite, constipation, and suicide risk in underage individuals, as well as nausea, tremors, and coma or seizures [14]. There are numerous case reports of cardiac and neurologic toxicities and serotonin syndrome in overdose. Even death from overdose has been reported [15]. However, it is still one of the most prescribed antidepressant drugs [16].

Quantitative determination of paroxetine and citalopram in human fluids and the environment is of practical importance for diagnosis, monitoring of disease [17], and optimization of therapeutic interventions of depression, as it may explain a non-response or adverse effects [1] and reduce unnecessary fatality cases among highly depressed patients resulting from hepatotoxicity and other drug-related issues [18].

Paroxetine and citalopram have been previously determined in pharmaceutical compounds and some real samples using spectroscopic [8] and chromatographic techniques [11]. The reported methods have many shortcomings such as potential loss of drugs in the re-extraction process, need of lengthy, tedious, and time-consuming plasma sample preparation and extraction process [19] as well as very low detection limits, expensive to perform procedures, and the need for trained expert personnel to complete complicated operations and the use of bulky instruments that have limited portability and make them inconvenient and unreliable for rapid detection and everyday use or on-site measurements [20].

Electrochemical sensors possess the desired characteristics for on-site measurement, and thus their application in the analysis of drugs, pharmaceuticals, and biological samples has increased greatly over the last few years [21]. Owing to the electroactive properties of SSRIs, electrochemical methods have been used for the detection of these drugs, providing adequate insight into the redox properties and metabolism of these compounds [22].

A typical electrochemical sensor is thought to consist of a sensing working electrode, a reference electrode and a counter electrode, all separated from each other by a layer of liquid electrolyte [23].

With a conventional bare or unmodified working electrode, the electrochemical detection of SSRIs may incur common problems, which include a low detection of SSRIs in real samples because of the low concentration of the analytes, the high overpotential at the working electrodes, as well as the interference of other biomolecules present in the sample having similar oxidation potential. Considering that SSRIs are adsorbed onto the surface of the electrode during the oxidation/reduction reactions, the reproducibility and reuse of the bare electrode are limited. The performance of electrodes in electrochemical methods can be improved by surface modification with various nanomaterials [24].

Nanomaterials are one of the most promising supporting materials for surface modification of electrodes, due to their unique properties such as good biocompatibility, high surface-to-volume ratio [25], substantial mechanical power and electrical and electrocatalytic properties [26]. These properties accelerate the rate of heterogeneous electron exchange between the nanomaterial-based electrode surface and the analyte of interest in solution and increase the effective surface area of the working electrode [27]. Iridium nanoparticles (IrNPs) and gold nanoparticles (AuNPs), owing to the nanoscale dimensions at the electrode surface, increase the effective surface area of the electrode [28]. Furthermore, the electrocatalytic properties of these nanoparticles facilitate electron transfer and increase the electrode sensitivity to the target species. The combination of the two nanoparticles with electrocatalytic properties develops electroactive composites that, as modifiers, can enhance the electrochemical sensitivity of the electrode and its overall performance. Moreover, as the sensitivity of detection in nanomaterial-based sensors is enhanced, probe materials are required at extremely low concentrations. By tuning the surface properties of the nanomaterials, these sensors can be easily employed for selective and specialized detection. An efficient detection system can help manage many problems in our modern-day lives. Sensors not only provide simple sample handling but also enable rapid analysis with higher sensitivity and better accuracy [19].

In the current study, a novel technique is developed by modifying a glassy carbon electrode (GCE) with an iridium-gold nanocomposite (IrAuNPs) on its surface, termed IrAu-GCE, to serve as a highly sensitive and selective electrochemical sensor for estimating paroxetine and citalopram. The electrochemical behaviours of paroxetine and citalopram at the IrAu-GCE were studied using cyclic voltammetry (CV) and square wave voltammetry (SWV). To appraise the efficacy of the modified electrode for analytical uses, it was applied for the voltametric determination of paroxetine and citalopram in real samples such as urine. The success of this study illustrates the potential for prompt point-of-care measurements of biological samples among depression patients diagnosed whose conditions seem worse even after being placed on treatment regimes.

Experimental

Materials and reagents

Dark horse coffee (coffee arabica) roasted capsules were purchased from local vendors in Cape Town, South Africa, hydrogen tetrachloroaurate (III) hydrate ($HAuCl_4{\cdot}3H_2O$), Sodium dihydrogen phosphate (NaH_2PO_4), disodium hydrogen phosphate (Na_2HPO_4), sulfuric acid (H_2SO_4) and ethanol (99.9 *%*) were obtained from Sigma Aldrich (Cape Town, South Africa), hydrochloric acid was purchased from Amresco (Ohio). All electrochemical experiments were carried out using a 0.1 M phosphate buffer (PB) solution with pH of 7.4 as electrolyte. Alumina polishing pads and powder (0.05, 0.3 and 1.0 micron) were obtained from Buehler (Illinois, USA). Ultra-pure water by a Milli-QTM system (Millipore) was used in all aqueous solutions and throughout the experiments.

Coffee waste extract preparation

Coffee waste was extracted by the espresso method, where the coffee grounds were then collected, washed and dried in an oven at 65 ℃. To the coffee ground, boiled, double-distilled water was added and left to stir at 65 ℃ for 1 hour. The coffee waste extract (CWE) was centrifuged at 10,000 rpm for 20 minutes and the resultant supernatant was then filtered using Whatman 0.4-micron filter paper. The filtrate was collected, kept at -80 °C overnight, and then lyophilized using the lyophilizer. The extracts were stored in a desiccator at room temperature for further experiments.

Synthesis of iridium nanoparticles

Iridium nanoparticles (IrNPs) were prepared with iridium chloride hydrate ($IrCl_3xH_2O$). The optimum conditions of IrNPs synthesis were tested. Among the variables, 5 mM $IrCl_3$ with 12 mg ml^{-1} of CWE at a volume ratio of (1:2) and a pH adjustment to pH 10 using HCl, exposed at 65 ℃ for 2 hours, were ideal for IrNPs preparation.

Synthesis of gold nanoparticles

To determine the biogenesis of gold nanoparticles (AuNPs), hydrogen tetrachloroaurate (III) hydrate ($HAuCl_4$) was used as a precursor salt for their synthesis. The ideal conditions for AuNPs synthesis were 1 mM $HAuCl_4$ with 12 mg ml^{-1} of CWE at a volume ratio of (1:4) at 65 ℃ for 1 h.

Synthesis of iridium-gold nanoparticles

For the synthesis of iridium-gold nanocomposites (IrAuNPs), various conditions were tested to determine the optimum conditions of synthesis. Among the variables, 5 mM $IrCl_3$ and 1 mM $HAuCl_4$ with 12 mg ml^{-1} of CWE at a volume ratio of (1:2:2) and a pH adjustment to pH 10 using HCl, exposed at 65 ℃ for 2 hours, was ideal for IrAuNPs preparation. The synthesized IrAuNPs were purified by washing with distilled water followed by centrifugation at 10,000 rpm for 10 minutes to remove any unbound coffee waste phytochemicals. The purified nanoparticles were collected in pellet form, dried in an oven, and used for characterization.

Characterization of nanomaterials

The optical properties of synthesized IrNPs, AuNPs and IrAuNPs were characterized using the POLARstar Omega microplate reader (BMG Labtech, Cape Town, South Africa). The Zetasizer (Malvern Instruments Ltd., UK) using dynamic light scattering (DLS) was used to analyse the hydrodynamic size distribution, polydispersity index (PDI) and zeta potential (ZP) values. High-resolution transmission electron microscopy (HRTEM) obtained from the FEI Tecnai G^2 20 field-emission gun (Field Electron and Ion Company, Hillsboro, OR, USA) was used to characterize the morphology and the particle size distribution. Energy dispersive spectrum (EDX) using an EDAX liquid nitrogen cooled lithium doped silicon detector confirmed the elemental composition of the nanoparticles and selected area electron diffraction (SAED) analysis was also performed on the same samples using HRTEM. PerkinElmer spectrum one FTIR spectrophotometer (Waltham, MA, USA) was used to determine the functional groups.

Preparation of nanocomposite platforms

The electrochemical experiments were carried out with a three-electrode system comprising the glassy carbon electrode (GCE) as the working electrode with a surface area of 0.0201 cm^2, Ag/AgCl (3 M KCl) as the reference electrode and platinum wire as the counter electrode. All electrodes were obtained from Bioanalytical Systems (BASi) in West Lafayette, USA. GCE was mechanically cleaned with alumina slurry followed by electrochemical cleaning, which was carried out by cycling in a 1 M solution of sulfuric acid between the potentials of -1000 and 1500 mV or until a reproducible

voltammogram was obtained using cyclic voltammetry (CV) carried out on a PalmSens potentiostat (Palm Instruments BV, Netherlands). Onto the clean GCE surface, 5 µl of each nanomaterial was drop-casted and the electrode was dried in an oven at 50 °C. The resulting electrodes will be called Ir-GCE (Ir modified glassy carbon working electrode), Au-GCE (Au modified glassy carbon working electrode) and IrAu-GCE (IrAu modified glassy carbon working electrode).

Electrochemical measurements

IrAu-GCE was used for the electrochemical analysis of paroxetine (PRX) and citalopram (CIT). All measurements were carried out with 0.1 M phosphate buffer solution (PBs), pH 7.4, as the electrolyte. Cyclic voltammetry (CV) and square wave voltammetry (SWV) techniques were used for electrochemical measurements ranging from a potential of -0.2 to 1.4 V. CV was performed with an equilibration (*E*) time of 5 s and an *E* step of 0.00595 V. SWV had an equilibration time of 5 s, *E* step of 0.02 V and an amplitude of 0.05 V at a frequency of 10 Hz. SWV was the preferred method for detecting paroxetine and citalopram because it is a more sensitive technique. All measurements were performed at room temperature.

Results and discussion

Green synthesis and characterization of IrNPs, AuNPs and IrAuNPs

IrNPs, AuNPs and IrAuNPs were synthesized through the interaction of CWE, which acted as reducing and stabilizing agents, with hydrogen tetrachloroaurate (III) hydrate ($HAuCl_4{\cdot}3H_2O$) and iridium chloride (III) hydrate ($IrCl_3{\cdot}xH_2O$) at 65 °C. The initial confirmation of nanoparticle syntheses was achieved through visual observation of a purple-blue colour change in the reaction suspension for IrNPS and a red wine colour for AuNPs from brown (Figure 1a). These colour changes are characteristic of colloidal AuNP solution, which is a result of the collective oscillation of free conduction electrons or surface plasmon resonance (SPR) and were also observed in green chemical syntheses of IrNPs [29] and AuNPs [30] found in literature. An initial colour change from brown to grey was observed for the synthesis of the IrAuNPs. These optical changes confirmed the presence of the respective IrNPs, AuNPs and IrAuNPs and that the phytochemicals or/secondary metabolites present in the CWE could reduce metal ions to metal nanoparticles.

Ultraviolet-visible (UV-Vis) spectroscopy analysis of the purple blue (IrNPs), red (AuNPs) and grey (IrAuNPs) solutions confirmed the formation of nanoparticles with strong absorption bands in the visible region 500 to 600 nm. Observation of an absorption band in the mentioned wavelength is a distinct feature indicating the presence of IrNPs and AuNPs, respectively [30]. As is clearly seen in all three UV-Vis spectra (Figure 1b), IrNPs exhibited a maximum absorbance (λ_{max}) of 562±2 nm, AuNPs of 557±0.5 nm and IrAuNPs of 560±2 nm. The band generated by AuNPs was more symmetrical and sharper than that of IrNPs and IrAuNPs, which may be indicative of better uniformity in the size distribution of AuNPs. IrNPs exhibited a broader and weaker plasmon absorption band, which is characteristic of inhomogeneity due to the aggregation of particles. The aggregation of the IrNPs may be attributed to centrifugation during the washing step [31]. In all three NP samples, a minimum absorption tail was shown towards the near infrared region (NIR), which may be indicative of their stability and/or lack of anisotropic NPs. Figure 1c displays bimodal size distributions of colloidal IrNPs, AuNPs, and IrAuNPs using DLS analysis. In all cases, the peak intensity of the large particles was higher than the peak intensity of the small particles, which was expected since the particle size distribution based on the light-scattering intensity is greatly influenced by larger particles [32]. DLS characterization of IrNPs, AuNPs and IrAuNPs demonstrated hydrodynamic sizes of 94.63±5.66, 69.36±3.99

and 82.13±2.84 nm, respectively. In agreement with the distribution curves, the hydrodynamic size of AuNPs is smaller than that of IrAuNPs and IrNPs, and IrAuNPs is smaller than that of IrNPs.

The stability of the metal nanoparticles was determined by measuring the zeta potential (ZP), which is a key component for practical applications [33]. As shown in Figure 1d, IrNPs have an average ZP of -37.74 mV, AuNPs have a ZP of -24,8 mV, and IrAuNPs of -20,3 mV. These negative values of ZP indicate that the surfaces of the IrNPs, AuNPs and IrAuNPs are negatively charged, suggesting that these nanoparticles are relatively stable and dispersed due to repulsive forces. Biologic coatings from various biowaste materials can provide different zeta potentials. The high stability of the particles is attributed to the presence of bioactive components as capping agents [34].

A strong peak was generated around 3400 cm^{-1} in the FTIR spectra of the CWE and the synthesized IrNPs, AuNPs and IrAuNPs (Figure 1e). This peak may be attributed to the stretching vibration of inter-molecular polymeric bonded O-H and C-O groups, indicating the presence of hydroxyl and carboxylic groups [35]. Similarly, a sharp peak was observed at 2924.29 cm^{-1} for the CWE and at 2922.5 cm^{-1} for both AuNPs and IrAuNPs. This is related to the asymmetric stretching of the aliphatic C-H groups [36]. Peaks at 1685.60, 1629.15, 1696.00 and 1633.98 cm^{-1} revealed C=O stretching of flavonoids/phenolic groups and N-H stretching (1˚amines, 2˚amines) [37]; C-N stretching mode at 1587.80 and 1408.92 cm^{-1}; -C-O-H bending, S=O (Sulfones, sulfonates); C-N (alcohols; carboxylic acid, esters, ethers) and C-H (alkyl halides) at 1261.83 cm^{-1} [38] and -C-O-C stretching in ethers, alcohols and polyphenols at 1075.00, 1098.85 and 1104.28 cm^{-1}. The transmittance of O-H and C-O bands on IrNPs, AuNPs and IrAuNPs may be due to the involvement of flavonoids, phenolic compounds, terpenoids and/or carbohydrates in the biosynthesis of these nanoparticles. Researchers in several studies have reported that these hydroxyls and carbonyl-containing compounds play a role in the reduction, capping and stabilization of the metallic NPs.

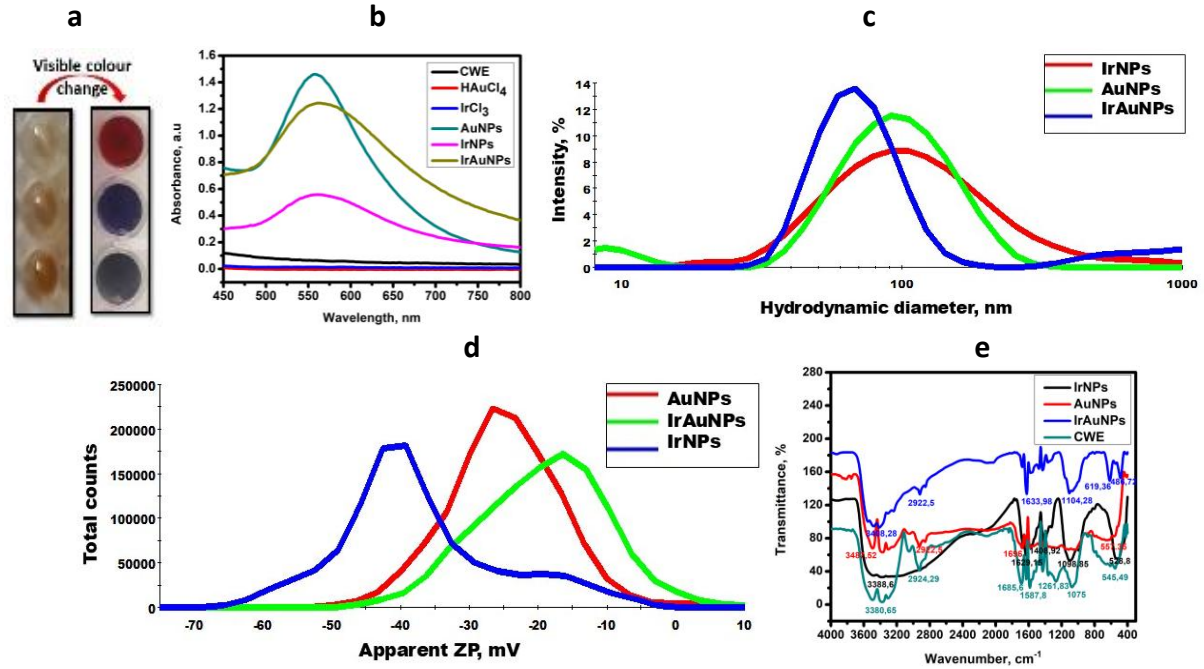

Figure 1. *(a) Changes in the color indicative of IrNPs, AuNPs and IrAuNPs synthesis, (b) UV-Vis spectra and distribution curves displaying the (c) hydrodynamic diameter and (d) ZP, (e) FTIR spectra of CWE, IrNPs, AuNPs and IrAuNPs*

HRTEM image in Figure 2.1a reveals the existence of IrNPs exhibiting a spherical shape with particles exhibiting a uniform morphology and good monodispersity and a few particles aggregating to form nanoclusters in the 5 nm range [39]. AuNPs illustrated particles exhibiting an assortment of geometric shapes that were mostly spherical and relatively monodispersed with good lattice fringes

in Figure 2.2a. The smaller detected particles had nearly spherical shapes, while larger particles exhibited pentagons, hexagons, triangles, and truncated triangles shapes [40]. The micrograph image of IrAuNPs in Figure 2.3a revealed small spherical particles with larger spherical, pentagon, hexagon, triangle, and truncated triangle-shaped particles. The particles of IrAuNPs are a combination of the morphology of IrNPs and AuNPs.

The particle size range of IrNPs was between 0 and 3 nm, with the largest number of particles between 2 and 2.2 nm in diameter (Figure 2.1b). The core diameter of IrNPs was found to be 2.05±0.43 nm, which is typically the size of IrNPs [41]. AuNPs revealed a particle size range of 0 and 55 nm, with the largest number of particles between 2 and 4 nm in diameter (Figure 2.2b). The core diameter of AuNPs was found to be 34.5±13.27 nm, which is typically the size of AuNPs [42]. In Figure 2.3b, the particle size range of IrAuNPs was between 0 and 18 nm, with the largest number of particles between 2 and 2.2 nm in diameter [35]. The core diameter of IrAuNPs was found to be 5.29±4.46 nm. These results are reflective of the DLS data. In DLS analysis, the capping agent of the nanoparticle is considered in the hydrodynamic diameter, whereas in HRTEM, the electron beam does not measure carbon-based materials, so the core diameter is measured.

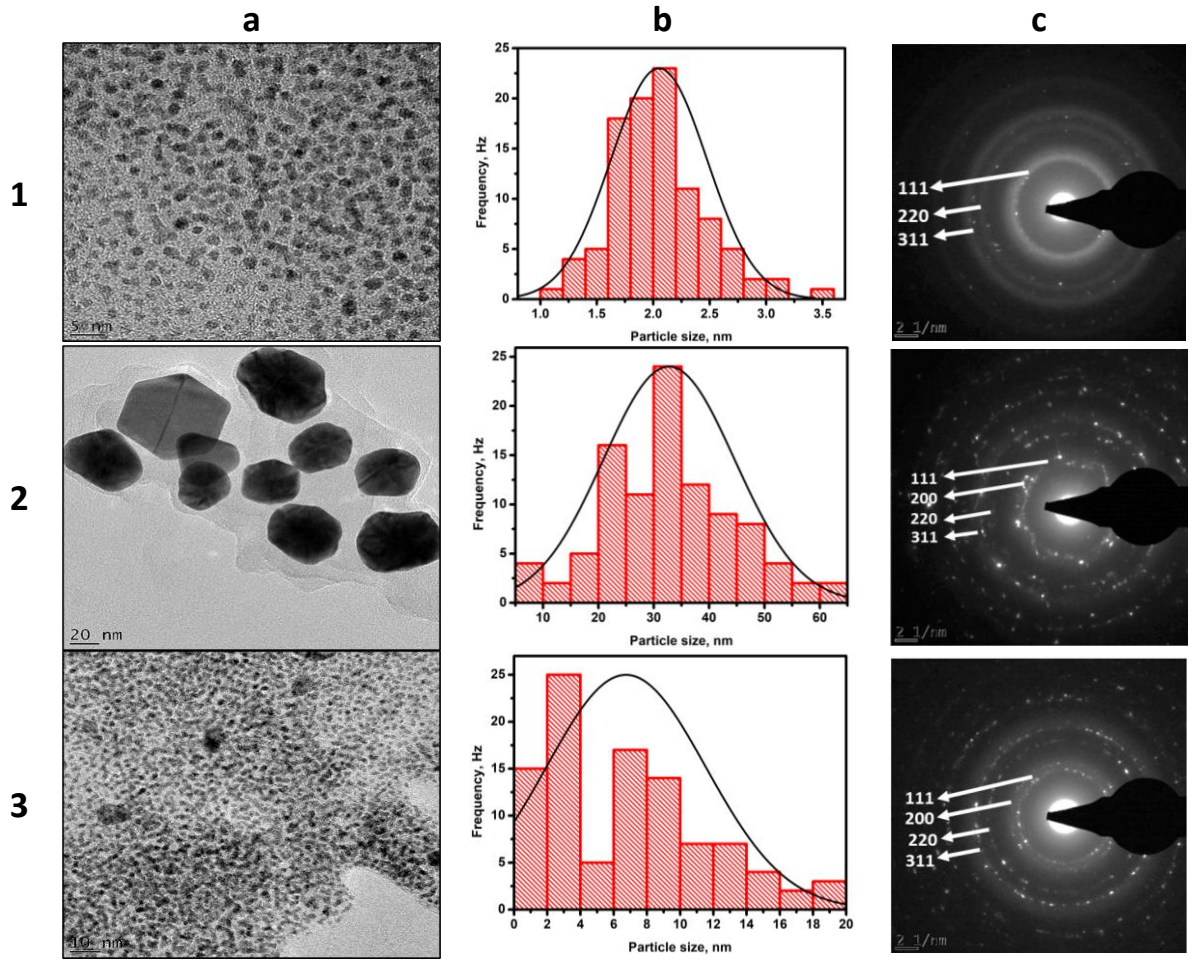

Figure 2. *HRTEM images of the respective IrNPs, AuNPs and IrAuNPs displaying the morphology (1a-3a), the size distribution (1b-3b), and the crystalline nature (1c-3c)*

The crystalline nature of the IrNPs, AuNPs and IrAuNPs was confirmed by the selected area electron diffraction (SAED). In Figure 2.1c, the identified Bragg reflections (bright rings) correspond to the (111), (220) and (311) sets of lattice planes, which can be indexed based on the face-centered cubic (FCC) structures of iridium as aligned by the arrows. Figure 2.2c also confirms that AuNPs is crystalline. Bragg reflections as indicated by arrows correspond to the (111), (200), (220) and (311)

sets of lattice planes of gold. IrAuNPs form crystalline structures as confirmed by the Bragg reflections as indicated by arrows, which correspond to the (111), (200), (220) and (311) sets of lattice planes, which are indexed on the FCC structures of both iridium and gold (Figure 2.3c).

Electrochemical behaviour of paroxetine and citalopram at GCE and IrAu-GCE

The electrochemical behaviour of PRX and CIT was investigated at the bare GCE and IrAu-GCE in 0.1 M PB (pH 7.4) under a nitrogen atmosphere to eliminate the presence of interfering oxygen molecules at the electrode surface [43] and the resultant peak currents were used for the quantitation of PRX and CIT.

SWV technique revealed oxidation peaks at 0.879 V for both PRX and CIT on the bare GCE, while no visible reduction peaks were present (Figure 3a and Figure 3b). These oxidation peaks are attributed to PRX [4] and CIT [44] and are in accordance with those found in the literature. This suggests that the oxidation of PRX and CIT is irreversible, or that the subsequent reduction of these drugs is difficult and may require more energy than that provided by the potentiostat [45]. The oxidation peaks for PRX and CIT could clearly be distinguished from the bare GCE in the absence of PRX and CIT, as GCEs are inherently chemically inert and present no attributed peaks in buffer [43]. For this purpose, the oxidation peaks were chosen to be monitored at 0.879 V for the detection of PRX and CIT, respectively. IrAuNPs on the GCE enhance the oxidation peak currents of the reactions of PRX (Figure 3a) and CIT (Figure 3b) compared to the bare GCE. At a concentration of 1 µM PRX, the GCE produced an anodic peak current (I_{pa}) of 2.293 µA at 0.879 V, whilst PRX at the IrAu-GCE yields an I_{pa} of 4.663 µA at 0.879 V. At a concentration of 20 µM CIT, the GCE produced an anodic peak current of 1.568 µA at 0.879 V, whilst CIT at the IrAu-GCE yields an I_{pa} of 2.530 µA at 0.969 V.

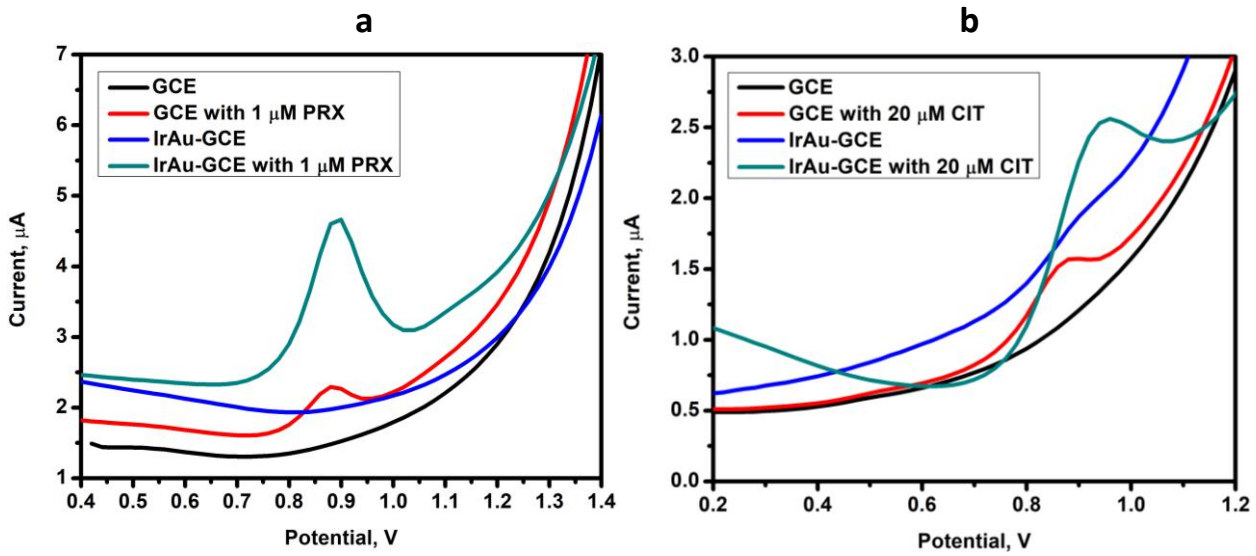

Figure 3. *Anodic SWVs in the absence and presence of (a) 1 µM PRX and (b) 20 µM CIT at bare GCE and IrAu-GCE in 0.1 M PB (pH 7.4)*

These large increases in peak current density are facilitated by a greater electron transport [16] brought about by the electroactivity and catalytic properties of IrAuNPs on the GCE surface [46]. The nanocomposite thus acts as an effective electrocatalyst for the respective detection of PRX and CIT, resulting in a current increase of nearly 2- to 3-fold. This electrocatalytic behaviour of IrAuNPs could be due to its large surface area, catalytic metal center, or active sites, and enhanced electrical conductivity, all of which aid in the oxidation of PRX and CIT [47].

Influence of accumulation potential and time

The experimental performance of IrAu-GCE towards the detection of PRX and CIT was maximized by testing the effect of accumulation potential and accumulation time on the oxidation peak current of 10 µM PRX and 20 µM CIT in 0.1 M PB (pH 7.4). The oxidation peak current was compared after 90 seconds of accumulation at different potentials from -1 to 0.6 V. The results show that the accumulation potential of -0.2 V for PRX (Figure 4a) and -1 V for CIT (Figure 4b) displayed the greatest peak current, but based on the consistency of the peak current produced, -0.2 V was selected as the optimum accumulation potential.

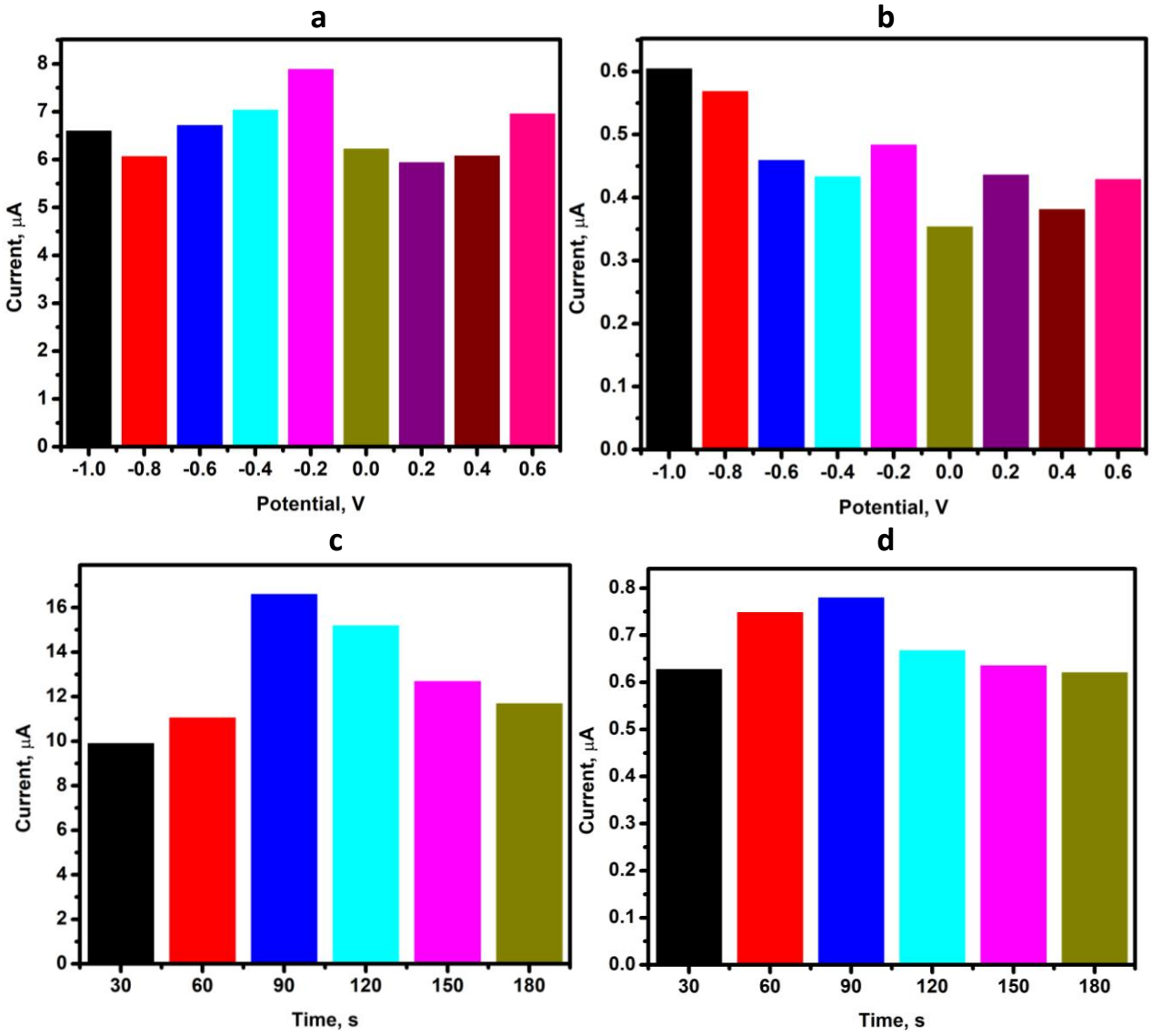

Figure 4*. Bar graphs of the average peak current versus accumulation potential (up) and accumulation time (down) of IrAu-GCE in 0.1 M PB (pH 7.4) containing (a,c) 10 µM PRX and (b,d) 20 µM CIT*

As observed in Figure 4c and Figure 4d, the oxidation peak current increases greatly within the first 90 seconds, reaching its optimum peak and due to the saturation of the electrode [48], the current then levels off. This accumulation time of 90 seconds causes the metallic ions to be reduced more completely, leading to higher peak currents. However, when the accumulation time is extended, the reduced ions cover the entire effective surface of the electrode, causing saturation for the IrAu platform and hence a decrease in the peak current response. These results reveal that IrAu-GCE exhibits effective accumulation at 90 seconds for PRX and CIT detection and thus it was

selected as the optimum accumulation time, as it combines good sensitivity and relatively short analysis time and was used throughout.

Electrochemical detection of paroxetine and citalopram

The relationship between the anodic peak current and the concentrations of PRX and CIT was studied at the bare GCE and at the IrAu-GCE. SWV was carried out in a potential window of -0.2 to 1.4 V to detect PRX and CIT in a phosphate buffer at pH 7.4, in the presence of oxygen, to mimic real conditions in which the sensor could be applied.

With the respective addition of 20 nM PRX and 1 µM CIT, the oxidation peaks appear at 0.899 V (Figure 5a) and 0.919 V (Figure 6a), which is attributed to the drugs being electro-catalysed by the IrAuNPs at the GCE surface. With the further increase in the analyte concentration, the anodic peak potential (E_{pa}) shifted anodically from 0.899 to 0.919 V for PRX and from 0.919 to 0.939 V for CIT and the oxidation peak currents gradually increased.

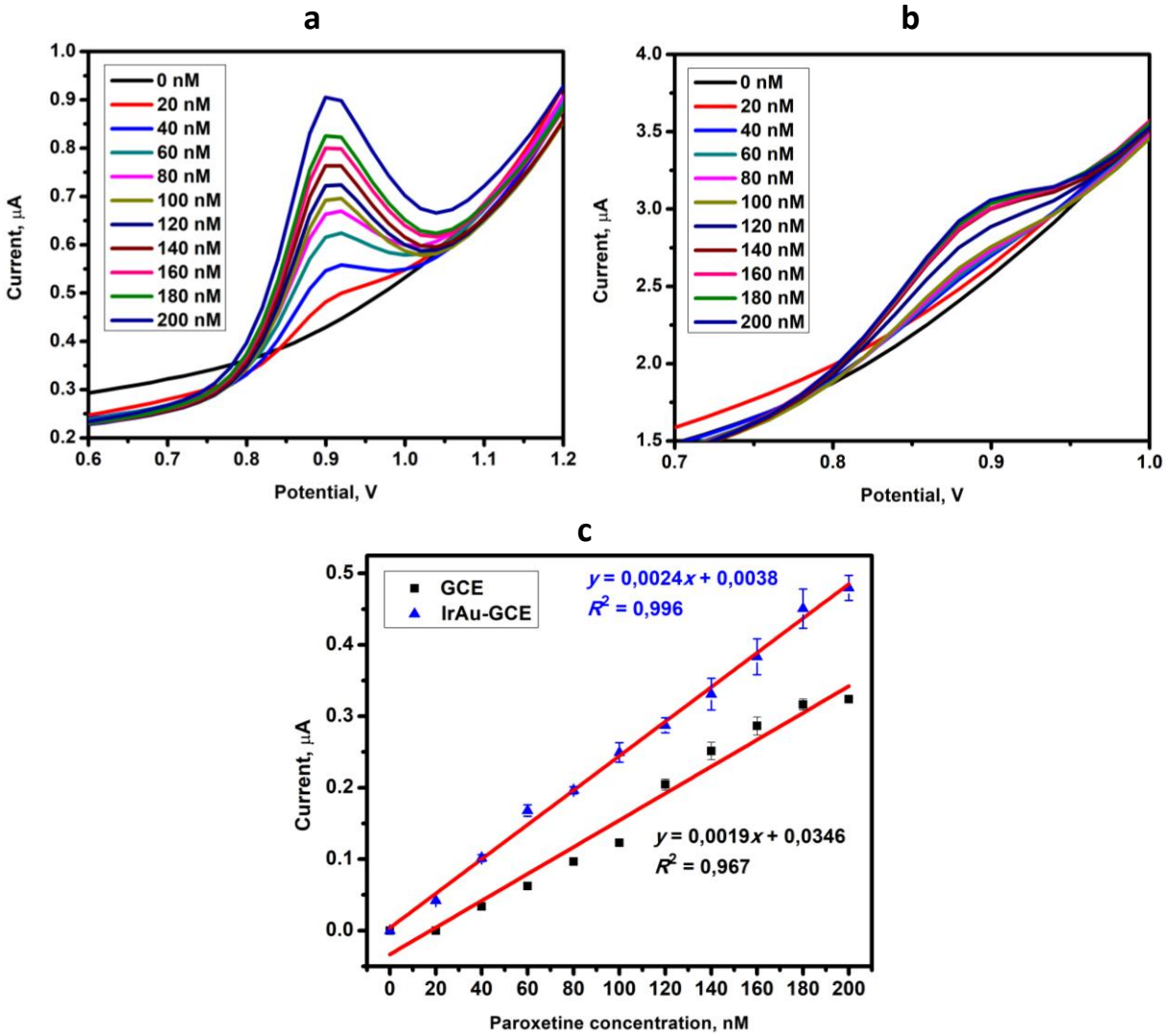

Figure 5. *SWV detection of paroxetine (0 to 200 nM) at (a) IrAu-GCE and (b) GCE surface in 0.1 M PB (pH 7.4), and (c) linear calibration plots of peak currents versus concentration of PRX*

Calibration graphs reveal that the detection of PRX was linear in the range of 20 to 200 nM with a correlation coefficient of R^2 = 0.996 and a sensitivity of 0.0024 µA nM^{-1} (Figure 5c). The limit of detection (LOD) and limit of quantification (LOQ) were calculated using Equations (1) and (2):

$$LOD = 3.3\ \sigma / s \quad (2)$$

$$LOQ = 10\ \sigma / s \quad (3)$$

where σ is the standard deviation of blank samples and s is the slope of the regression equation. The values of these limits are LOD of 0.072 nM and LOQ of 0.240 nM for the detection of PRX. The detection of CIT was found to be linear in the range of 1 to 10 µM with a correlation coefficient of R^2 = 0.991 and a sensitivity of 0.035 µA µM^{-1} (Figure 6c). The LOD of 0.085 µM and LOQ of 0.285 µM for the detection of CIT at the IrAu-GCE were calculated.

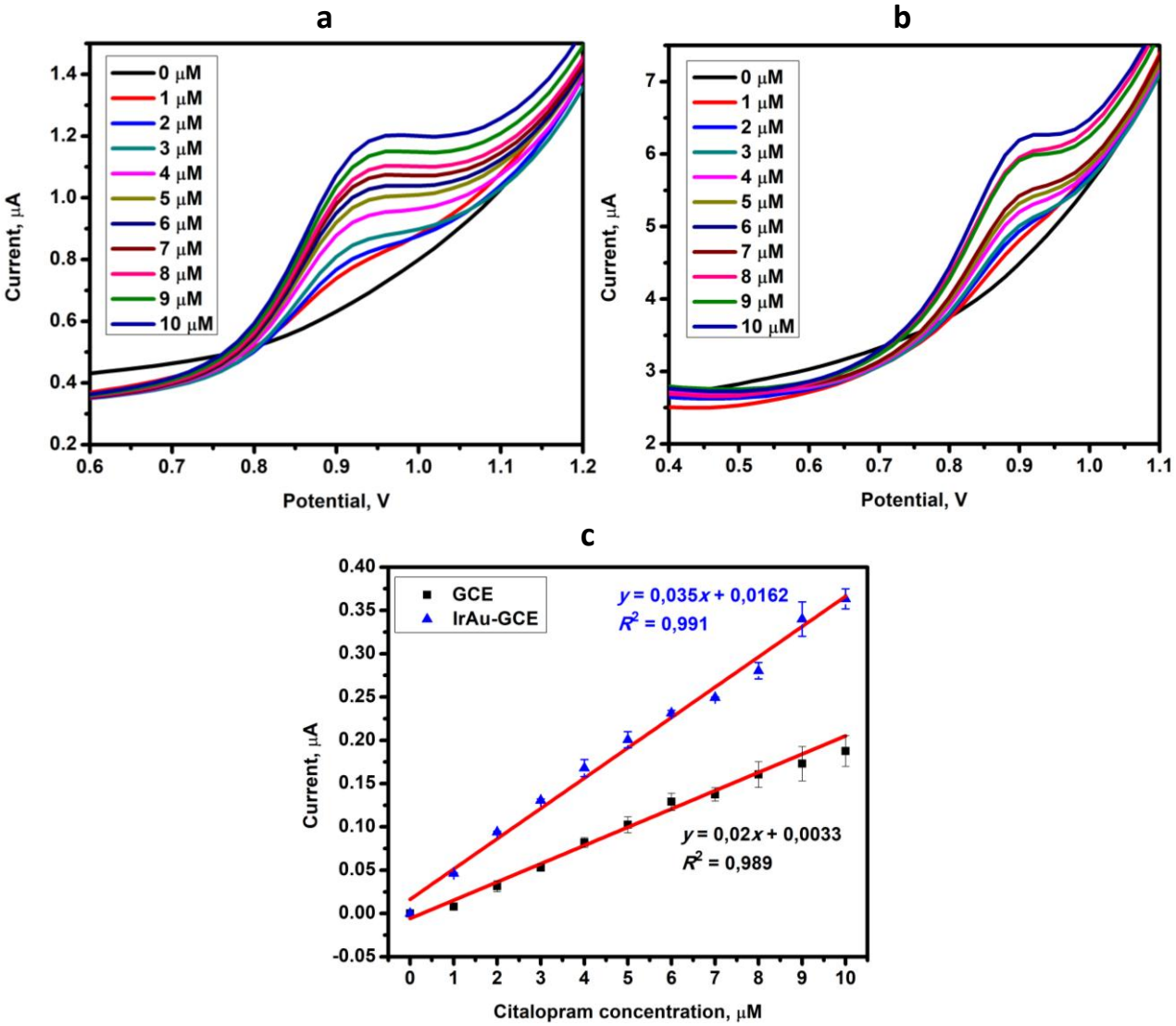

Figure 6. *SWV detection of CIT (0 to 10 µM) at (a) IrAu-GCE and (b) GCE surface in 0.1 M PB (pH 7.4) and (c) linear calibration plots of peak currents versus concentration of CIT*

In a comparative study, bare GCE was used to detect PRX concentrations ranging from 20 to 200 nM (Figure 5b) and CIT concentrations from 1 to 10 µM (Figure 6b).

GCE was unable to detect 20 nM of PRX, and the peak potential shifted anodically with increased concentration from 0.879 to 0.899 V (Figure 5b). With the addition of 1 µM CIT, the oxidation peak appeared at 0.895 V and the peak potential shifted anodically from 0.895 to 0.899 V with increased concentration from 1 to 10 µM (Figure 6b). The calibration plot for PRX exhibited a correlation coefficient of R^2 = 0.967 and a sensitivity of 0.0019 µA nM^{-1} with a LOD of 2.791 nM and LOQ of 9.304 nM in the linear range of 40 to 200 nM (Figure 5c). In Figure 6c, the calibration plot for CIT exhibited a correlation coefficient of R^2 = 0.989 and a sensitivity of 0.020 µA µM^{-1} with a LOD of 0.212 µM and

LOQ of 0.707 µM in the linear range of 1 to 10 µM. These values show an enhanced detection of these antidepressants at the modified electrode compared to the bare glassy carbon electrode.

The obtained values fall within the range reported by other researchers regarding PRX oxidation at the chemically modified electrode surface. However, this was not observed for the oxidation of CIT, where higher values were achieved at the chemically modified electrode surface. The linear range and detection limit of the developed electrochemical sensor, as two important analytical factors, are presented in Table 1 along with those reported previously for the measurement of PRX and CIT.

Table 1. *Analytical performance of IrAu-GCE and some previously reported electrodes for the detection of PRX and CIT*

Coating	Technique	Analyte	Linear range, µM	LOD, µM	Ref.
GCE/Nafion/MWCNT	DPV	Paroxetine	0.1 to 2.5	0.06	[45]
CSS-SPE[a]	SWV	Paroxetine	1 to 10	0.67	[49]
rGo/PWA/PGE[b]	DPV	Paroxetine	0.008 to 6	0.0009	[16]
MIPP,S/Sol-Gel/PWA/rGO/PGE[c]	adDPV[d]	Paroxetine	0.005 to 2.2	0.0007	[4]
Poly(DL-met)/AuNPs-GCE[e]	DPV, EIS[f]	Paroxetine	0.00005 to 100	0.00001	[50]
Au/PANSAPoly-2D6[g]	CV	Paroxetine	0.005 to 0.05	0.002	[51]
IrAu-GCE	SWV	Paroxetine	0.02 to 0.2	0.00007	Present work
Au-PdNPs-GR-AuE[h]	SWV, EIS	Citalopram	0.5 to 50	0.049	[52]
ZnO-MWCNT-CPE	ASWV[i]	Citalopram	0.012 to 1.54	0.005	[53]
Fe_3O_4@[(EtO)3Si-L]/MWCNTs-GCE[j]	DPV	Citalopram	0.3 to 10 000	0.0532	[44]
ZIP-8/g-C_3N_4/RGO-CPE[k]	DPV	Citalopram	0.1 to 10	0.05	[14]
P(pABSA)/β-CD/MWCNT-GCE[l]	EIS	Citalopram	0.09 to 100	0.044	[6]
JUK-2-MWCNTs-AuNPsGCE[m]	EIS	Citalopram	0.05 to 115	0.011	[38]
IrAu-GCE	SWV	Citalopram	1 to 10	0.085	Present work

[a]carbon spherical shells screen-printed electrode, [b]Polyoxometalate/reduced graphene oxide modified pencil, graphite [c]molecular imprinted polymer/sol-gel/polyoxometalate/rGO, [d]adsorptive DPV, [e]conducting polymer poly-methionine/gold nanoparticles-modified, [f]electrochemical impedance spectroscopy, [g]poly cytochrome P450-2D6 enzyme encapsulated in nanotubular poly (8-anilino-1-napthalene sulphonic acid) on gold, [h]gold-palladium bimetallic nanoparticles decorated graphene modified gold electrode, [i]adsorptive SWV, [j]core shell structured functionalized iron oxide nanoparticles with Schiff base ligand, [k]zeolite imidazolate framework on graphite carbon nitride zeolite imidazolate framework, [l]multiwall carbon nanotube/(poly(p-aminobenzene sulfonic acid)/β-cyclodextrin), [m]manganese-based metal-organic framework

In contrast to all the modified electrodes presented in Table 1, the fabricated IrAu-GCE is easy to construct and does not require the use of harmful solvents like DMF. Moreover, at all stages, from the synthesis of the IrAuNPs to the construction of the IrAu-GCE platform and the quantification of PRX and CIT, only reagents neutral for the environment were used, promoting the principles of green analytical chemistry. These results demonstrate that the IrAu-GCE exhibited enhanced detection of PRX, detecting lower concentrations of this antidepressant with a greater sensitivity of 0.0024 µA nM-1, a lower LOD of 0.072 nM, and an LOQ of 0.240 nM.

Precision studies: reproducibility and stability of sensor

To investigate the reproducibility of the IrAu-GCE, five electrodes were freshly prepared with IrAuNPs and used to measure 10 µM PRX and 20 µM CIT, respectively, in 0.1 M PB (pH 7.4) under optimum conditions. It was observed that the peak currents for PRX and CIT were almost constant with relative standard deviations (RSD) of 2.47 and 3.4 % respectively, determined by recording the peak current responses for five replicate measurements. IrAu-GCE demonstrated high reproducibility.

The stability of IrAu-GCE was tested by measuring the current response of 10 µM PRX and 20 µM CIT, respectively, in 0.1 M PB (pH 7.4) solution intermittently after being stored in dry conditions at 4 °C for seven consecutive days. There were no changes in the oxidation peak potentials for PRX and CIT at 4 °C, and the electrodes maintained a current response of 87.9 to 94.6 % for 4 °C (Figures 7a

and 7b) in comparison to the original responses, respectively. The sensor presented excellent stability, as shown by the current responses. These results revealed that the designed IrAu-GCE has suitable stability and reproducibility for practical applications in the detection of PRX and CIT.

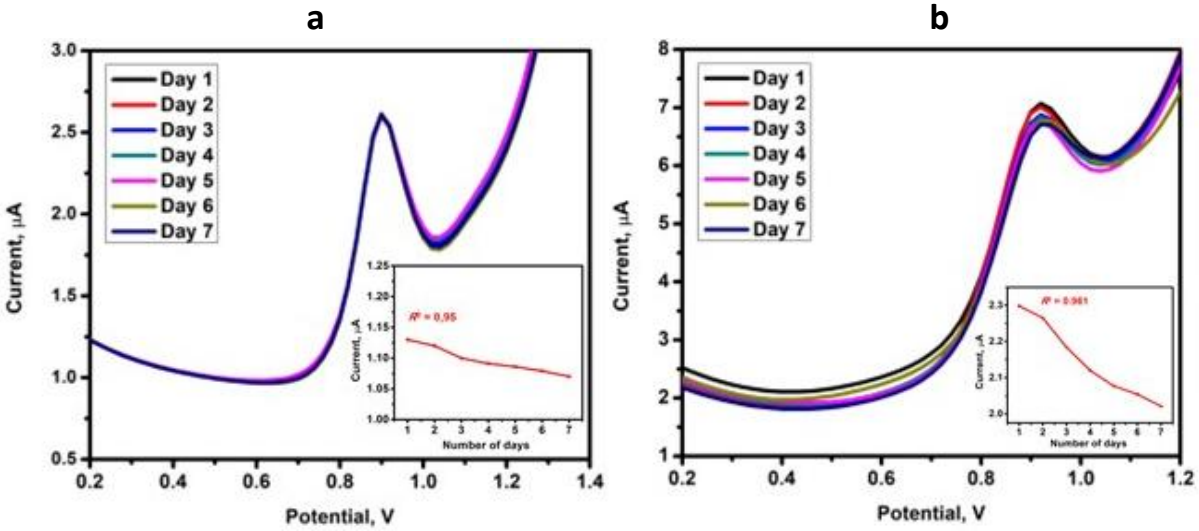

Figure 7. *SWVs of IrAu-GCE in 0.1 M PB (pH 7.4) containing (a) 10 µM PRX and (b) 20 µM CIT stored at 4 °C for seven (7) days, insets: plots of peak currents vs. number of days*

Selectivity: interference studies of IrAu-GCE

The analytical selectivity of sensors plays an important role in the analytical determination of drugs coexisting with common excipients and matrix complexity. To evaluate the selectivity of the method for the determination of PRX and CIT, the influence of potentially interfering substances such as acetaminophen (APAP), ascorbic acid (AA), caffeine, sertraline (STR), and dexamethasone (DEX) was evaluated. The maximum concentrations of these potential interfering species were taken as a tolerance limit that caused ±5 % relative error in the determination of PRX and CIT. In accordance with the data in Figure 8, AA (Figure 8.1b) and caffeine (Figure 8.1c) had no interference with the detection of PRX and CIT even at concentrations 3-fold higher than these analytes. APAP (Figure 8.2a) and DEX (Figure 8.2d) had no significant interference with CIT at concentrations 3-fold higher than CIT. APAP (Figure 8.1a), DEX (Figure 8.1d) and STR (Figure 8.1e) showed some interference with the detection of PRX, whilst STR (Figure 8.2e) showed some interference with the detection of CIT. PRX and CIT can be selectively determined in the presence of probable biological molecules and pharmaceutical species without any significant pretreatment steps. However, when used with other drugs or SSRIs, detecting PRX and CIT becomes difficult. This sensor, therefore, offers a selective determination of PRX and CIT in compounds found in human bodily fluids. This sensor is also very useful, and it can be optimized for the co-detection of other compounds.

Accuracy: real sample studies of IrAu-GCE

The analytical applicability and reliability of IrAu-GCE were investigated by the respective measurements of PRX and CIT in a more complex matrix, such as synthetic urine, by a standard addition method. Various concentrations of PRX and CIT were detected in 20 *%* synthetic urine, which was prepared in a 1:5 ratio with pH 7 PB.

The detection of PRX and CIT was carried out in 20 *%* synthetic urine in the concentration ranges of 2 to 20 µM (Figure 9a) and 10 to 55 µM (Figure 9c) using SWV. With the addition of PRX from 2 to 20 µM and CIT from 10 to 55 µM, the peak potentials at 0.899 and 1.059 V shifted anodically to 0.919 and 1.1 V, respectively.

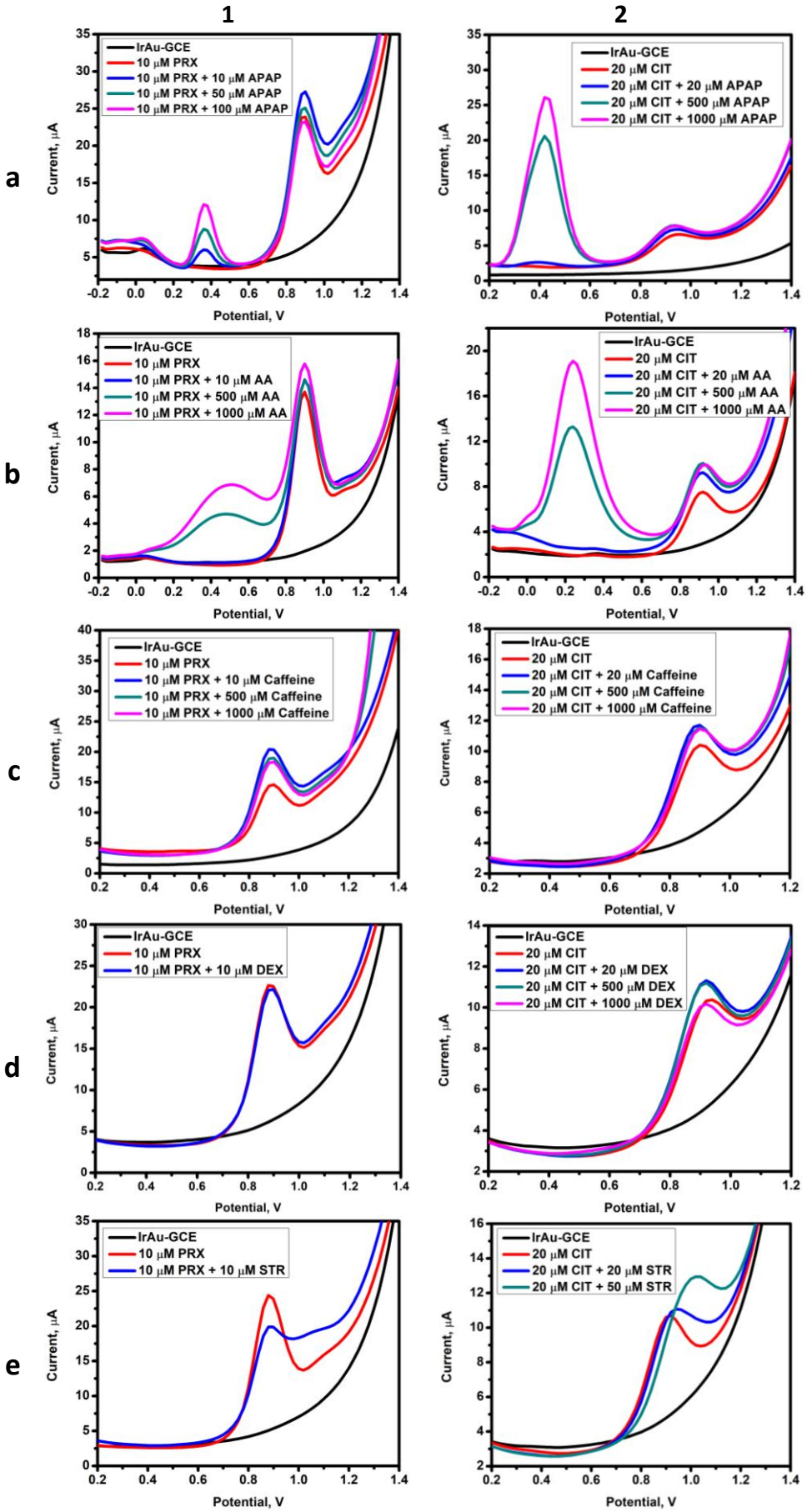

Figure 8. *SWVs of IrAu-GCE in 0.1 M PB (pH 7.4) containing (1) 10 μM PRX and (2) 20 μM CIT with: (a) APAP, (b) AA, (c) caffeine, (d) DEX and (e) STR as interfering substances*

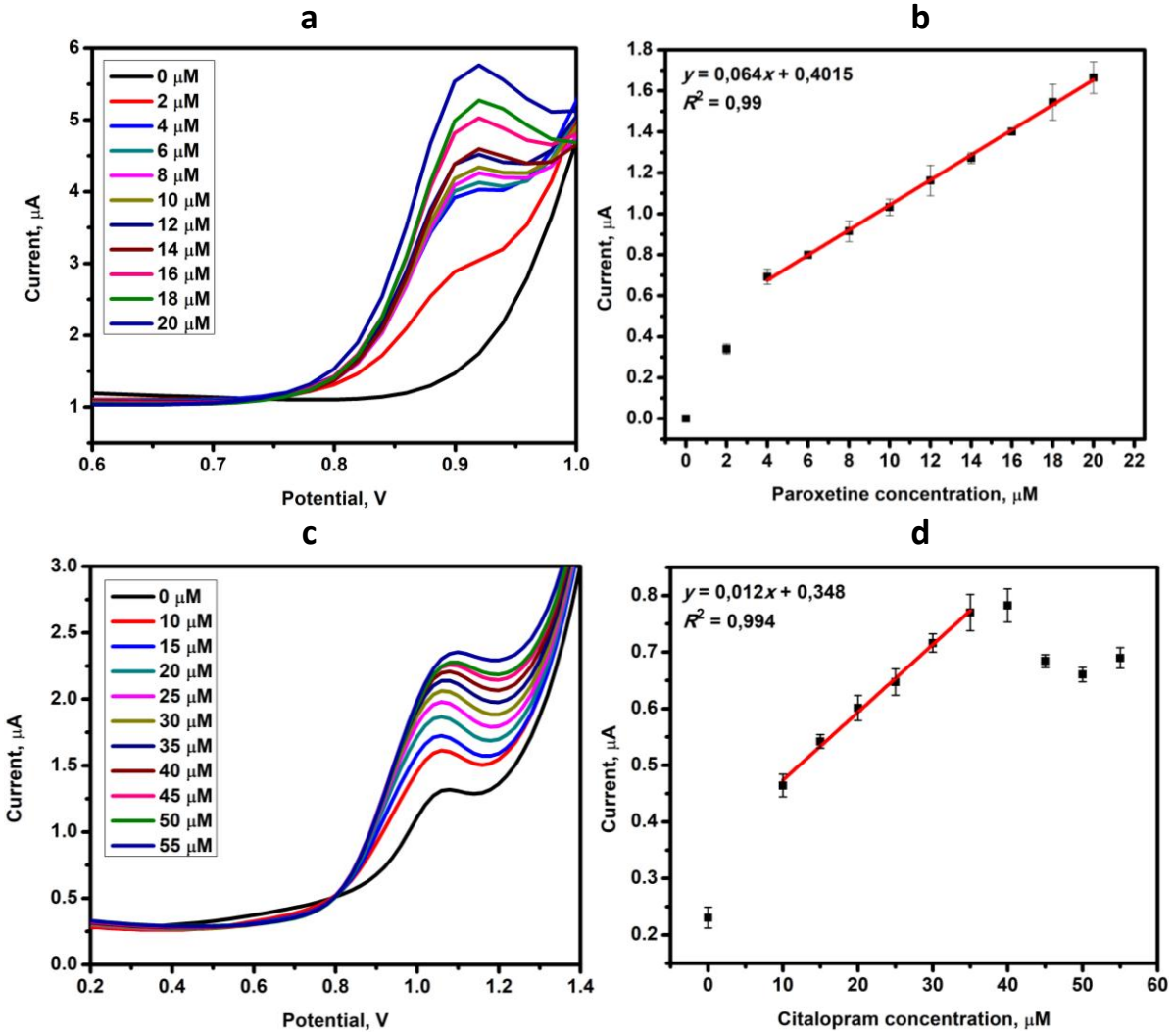

Figure 9. *SWV detection (a,c) and calibration plots of peak current versus concentration (b,d) of paroxetine (up) and citalopram (down) at IrAu-GCE in 20 % synthetic urine*

The resulting sensitivity was higher for synthetic urine compared to the sensitivity obtained for detecting PRX and CIT in PB within their respective ranges. The effect of synthetic urine on the linear range of the detection of PRX and CIT is quite greater compared to pure PB, with a greater sensitivity of 0.064 and 0.012 μA μM^{-1} (Figure 9b and Figure 9d). However, concentrations lower than 2 μM of PRX and 10 μM of CIT in the synthetic urine presented erratic responses and were not analytically feasible. The LOD was determined to be 1.168 μM for PRX and 5.669 μM for CIT, with a LOQ of 3.896 and 18.891 μM. The dynamic linear range was much higher in the case of synthetic urine than in the case of the buffer and this is due to the interfering substance that makes up urine.

Recovery studies of IrAu-GCE

The prepared IrAu-GCE sensor was used for recovery tests in synthetic urine. The 20 *%* synthetic urine sample was spiked with various amounts of PRX and CIT solutions and SWV was used to record the resultant responses. The amount of PRX and CIT in the urine solution was then calculated from the calibration plots (Figures 9b and 9d). The recovery of PRX and CIT was determined by comparing the peak currents of the drug in urine with those of pure PRX using the calibration plot in Figures 9b and 9c. It was observed that the recovery ranged from 90 to 115.1 *%* for PRX and 86 to 113.3 *%* for CIT. Based on the data obtained, it can be concluded that the fabricated modified chemical sensor represents acceptable recoveries for analytical applications.

Conclusions

In this work, IrAuNP was successfully synthesized from CWE and employed to modify GCE for the rapid and sensitive detection of PRX and CIT. The anodic peak currents of PRX and CIT showed enhanced responses at IrAu-GCE than at the bare GCE due to a greater electron transfer rate ensured by the electroactivity and catalytic properties of the nanocomposite. The electrocatalytic behaviour of IrAuNPs could be attributed to its large surface area, catalytic metal centres or active sites, and enhanced electrical conductivity, all of which aid in the oxidation of PRX and CIT. Under the optimized conditions, the IrAu-GCE displayed a low LOD of 0.072 nM and 0.085 µM in the linear ranges of 20 to 200 nM and 1 to 10 µM for PRX and CIT, respectively, with good sensitivity in a rapid analysis time of 90 seconds. The bimetallic nanocomposite electrochemical sensor showed excellent recovery of 86 and 115.1 *%* for the analytes in urine, with good stability performance of 87.8 to 94.6 *%* over a period of 7 days. The reproducibility of paroxetine and citalopram detection was plausible with RSD of 2.47 to 3.4 *%*. The results of this study suggest that the IrAu-GCE is suitable for the selective determination of PRX and CIT in real samples such as urine. The electrochemical sensor provides a portable and easy-to-use mode of detection, enabling point-of-care analysis and rapid response time. This sensor can thus be successfully applied as a form of therapeutic drug monitoring during antidepressant treatment to minimize the adverse drug reactions brought on by the treatment of the disease.

Acknowledgements*: The authors would like to express their gratitude to the National Research Foundation (NRF), South Africa, for funding this research study. The authors gratefully acknowledge the exceptional support and encouraging research environment provided by the management of SensorLab Laboratories, the Department of Chemistry and the Molecular Sciences and Biochemistry Laboratory at the University of the Western Cape.*

References

[1] R. Das, Y. K. Agrawal, Trends and Advances in Separation and Detection of SSRIs and SNRIs in Biological Matrices, *Chromatography Research International* **2013** (2013) 139459. https://doi.org/10.1155/2013/139459

[2] Z. Pan, C. Park, E. Brietzke, H. Zuckerman, C. Rong, R. B. Mansur, D. Fus, M. Subramaniapillai, Y. Lee, R.S. McIntyre, Cognitive impairment in major depressive disorder, *CNS Spectrums* **24** (2019) 22-29. https://doi.org/10.1017/S1092852918001207

[3] M. Feroz, I.C. Lopes, H. ur Rehman, S. Ata, P. Vadgama, A novel molecular imprinted polymer layer electrode for enhanced sensitivity electrochemical determination of the antidepressant fluoxetine, *Journal of Electroanalytical Chemistry* **878** (2020) 114693. https://doi.org/10.1016/j.jelechem.2020.114693

[4] A. Hassan Oghli, A. Soleymanpour, Ultrasensitive electrochemical sensor for simultaneous determination of sumatriptan and paroxetine using molecular imprinted polymer/sol-gel/polyoxometalate/rGO modified pencil graphite electrode, *Sensors Actuators B* **344** (2021) 130215. https://doi.org/10.1016/j.snb.2021.130215

[5] N. Naz, S. N. Ali, A. Qayoom, S. Iqbal, S. Akram, Rapid and sensitive method for simultaneous determination of citalopram with antihistamines by liquid chromatography, *Pakistan Journal of Pharmaceutical Sciences* **34** (2021) 835-841. https://doi.org/10.36721/PJPS.2021.34.3.REG.835-841.1

[6] M. B. Gholivand, A. Akbari, A novel voltammetric sensor for citalopram based on multiwall carbon nanotube/(poly(p-aminobenzene sulfonic acid)/β-cyclodextrin), *Material Science and Engineering: C* **62** (2016) 480-488. https://doi.org/10.1016/j.msec.2016.01.066.

[7] F. Faridbod, N. Davarkhah, S. Karamdoust, All solid sate potentiometric sensors for the measurement of paroxetine in pharmaceutical formulation, *International Journal of Electrochemical Science* **10** (2015) 8308-8320. https://doi.org/10.1016/S1452-3981(23)11097-2

[8] R. Nimal, D. Nur Unal, C. Erkmen, S. Kurbanoglu, M. Siddiq, G. Eren, A. Shah, B. Uslu, Elucidating the interaction of antidepressant drug paroxetine with ct-dsDNA: A comparative study by electrochemical,

spectroscopic, and molecular docking approaches, *Bioelectrochemistry* **149** (2023) 108285. https://doi.org/10.1016/j.bioelechem.2022.108285

[9] Y. Ma, C. Wang, S. Luo, B. Li, T. D. Wager, W. Zhang, Y. Rao, S. Han, Serotonin transporter polymorphism alters citalopram effects on human pain responses to physical pain, *Neuroimage* **135** (2016) 186-196. https://doi.org/10.1016/j.neuroimage.2016.04.064

[10] C. Ran, H. Zhou, C. Tan, J. Tan, Z. Zhang, W. Zhao, Detection and Evaluation of Adverse Drug Reaction Signals of Antidepressants Based on FDA Adverse Event Reporting System Database, *Open Journal of Depression* **09** (2020) 17-25. https://doi.org/10.4236/ojd.2020.92002

[11] P. Magalhães, G. Alves, A. Llerena, A. Falcão, Therapeutic drug monitoring of fluoxetine, norfluoxetine and paroxetine: A new tool based on microextraction by packed sorbent coupled to liquid chromatography, *Journal of Analytical Toxicology* **41** (2017) 631-638. https://doi.org/10.1093/jat/bkx043

[12] A. Roszkowska, A. Plenis, P. Kowalski, T. Bączek, I. Olędzka, Recent advancements in techniques for analyzing modern, atypical antidepressants in complex biological matrices and their application in biomedical studies, *TrAC Trends in Analytical Chemistry* **152** (2022) 116609. https://doi.org/10.1016/j.trac.2022.116609

[13] S. L. Aldrich, E. A. Poweleit, C. A. Prows, L. J. Martin, J. R. Strawn, L. B. Ramsey, Influence of CYP2C19 metabolizer status on escitalopram/citalopram tolerability and response in youth with anxiety and depressive disorders, *Frontiers in Pharmacology* **10** (2019) 99. https://doi.org/10.3389/fphar.2019.00099

[14] M. H. Karimi-Harandi, M. Shabani-Nooshabadi, R. Darabi, Simultaneous determination of citalopram and selegiline using an efficient electrochemical sensor based on ZIF-8 decorated with RGO and g-C3N4 in real samples, *Analytica Chimica Acta* **1203** (2022) 339662. https://doi.org/10.1016/j.aca.2022.339662

[15] G. Mannocchi, R. Tittarelli, F. Pantano, F. Vernich, M. Pallocci, P. Passalacqua, M. Treglia, L. T. Marsella, Forensic Aspects of a Fatal Intoxication Involving Acetaminophen, Citalopram and Trazodone: A Case Report, *Toxics* **10** (2022) 486. https://doi.org/10.3390/toxics10080486

[16] A. H. Oghli, A. Soleymanpour, Polyoxometalate/reduced graphene oxide modified pencil graphite sensor for the electrochemical trace determination of paroxetine in biological and pharmaceutical media, *Materials Science and Engineering C* **108** (2020) 110407. https://doi.org/10.1016/j.msec.2019.110407

[17] J. Xu, J. Tao, L. Su, J. Wang, T. Jiao, A critical review of carbon quantum dots: From synthesis toward applications in electrochemical biosensors for the determination of a depression-related neurotransmitter, *Materials (Basel)* **14** (2021) 3987. https://doi.org/10.3390/ma14143987

[18] K. Murtada, F. de Andrés, M. Zougagh, Á. Ríos, Strategies for antidepressants extraction from biological specimens using nanomaterials for analytical purposes: A review, *Microchemical Journal* **150** (2019) 104193. https://doi.org/10.1016/j.microc.2019.104193

[19] M. Brycht, S. Skrzypek, N. Karadas-Bakirhan, S. Smarzewska, B. Bozal-Palabiyik, S. A. Ozkan, B. Uslu, Voltammetric behavior and determination of antidepressant drug paroxetine at carbon-based electrodes, *Ionics (Kiel)* **21** (2015) 2345-2354. https://doi.org/10.1007/s11581-015-1390-6

[20] A. A. Abu-hassan, M. A. Omar, S. M. Derayea, Use of acetylacetone for nano-level assay of fluvoxamine maleate in pure form and pharmaceutical formulation, *Luminescence* **35** (2020) 1360-1365. https://doi.org/10.1002/bio.3898

[21] A. G. dos Santos Neto, C. S. de Sousa, A. da Silva Freires, S. M. Silva, H. Zanin, F. S. Damos, R. de Cássia Silva Luz, Electrochemical sensor for detection of imipramine antidepressant at low potential based on oxidized carbon nanotubes, ferrocenecarboxylic acid, and cyclodextrin: application in psychotropic drugs and urine samples, *Journal of Solid State Electrochemistry* **22** (2018) 1385-1394. https://doi.org/10.1007/s10008-017-3772-3

[22] F. C. O. L. Martins, L. C. Pimenta, D. De Souza, Antidepressants determination using an electroanalytical approach: A review of methods, *Journal of Pharmaceutical and Biomedical Analysis* **206** (2021) 114365. https://doi.org/10.1016/j.jpba.2021.114365

[23] T. T. T. Tran, D. M. Nguyen, A. Q. Dao, V. T. Le, Y. Vasseghian, A state-of-the-art review on the nanomaterial-based sensor for detection of venlafaxine, *Chemosphere* **297** (2022) 134116. https://doi.org/10.1016/j.chemosphere.2022.134116

[24] S. Sharma, N. Singh, V. Tomar, R. Chandra, A review on electrochemical detection of serotonin based on surface modified electrodes, *Biosensors and Bioelectronics* **107** (2018) 76-93. https://doi.org/10.1016/j.bios.2018.02.013

[25] W. Jin, G. Maduraiveeran, Nanomaterial-based environmental sensing platforms using state-of-the-art electroanalytical strategies, *Journal of Analytical Science and Technology* **9** (2018) 18. https://doi.org/10.1186/s40543-018-0150-4
[26] A. K. Attia, M. A. Mohamed, A. M. Fekry, Electroanalytical determination of escitalopram oxalate using nickel nanoparticles modified carbon paste sensor, *Acta Chimica Slovenica* **64** (2017) 415-421. https://doi.org/10.17344/acsi.2017.3193
[27] M.A . Sultan, A. K. Attia, M. M. Abou El-Alamin, M. A Atia, The novel use of multiwalled carbon nanotubes based sensors for voltammetric determination of itraconazole: application to pharmaceutical dosage form and biological samples through spiked urine samp, *World Journal of Pharmacy and Pharmaceutical Sciences* **5** (2016) 93-108. https://www.researchgate.net/profile/Ali-Attia3/publication/305851485
[28] J. M. Pingarrón, P. Yáñez-Sedeño, A. González-Cortés, Gold nanoparticle-based electrochemical biosensors, *Electrochimica Acta* **53** (2008) 5848-5866 https://doi.org/10.1016/j.electacta.2008.03.005
[29] Y. Zhao, E. A. Hernandez-Pagan, N. M. Vargas-Barbosa, J. L. Dysart, T. E. Mallouk, A high yield synthesis of ligand-free iridium oxide nanoparticles with high electrocatalytic activity, *The Journal of Physical Chemistry Letters* **2** (2011) 402-406. https://doi.org/10.1021/jz200051c
[30] Z. Wei, K. Luciano, X. Xia, Catalytic Gold-Iridium Nanoparticles as Labels for Sensitive Colorimetric Lateral Flow Assay, *ACS Nano* **16** (2022) 21609-21617. https://doi.org/10.1021/acsnano.2c10574
[31] G. Ghodake, C.Y. Eom, S. W. Kim, E. Jin, Biogenic nano-synthesis; Towards the efficient production of the biocompatible gold nanoparticles, *Bulletin of the Korean Chemical Society* **31** (2010) 2771-2775. https://doi.org/10.5012/bkcs.2010.31.10.2771
[32] A. M. Elbagory, C. N. Cupido, M. Meyer, A. A. Hussein, Large scale screening of southern African plant extracts for the green synthesis of gold nanoparticles using microtitre-plate method, *Molecules* **21** (2016) 1498. https://doi.org/10.3390/molecules21111498
[33] M. Cui, Y. Zhao, C. Wang, Q. Song, Synthesis of 2.5 nm colloidal iridium nanoparticles with strong surface enhanced Raman scattering activity, *Microchimica Acta* **183** (2016) 2047-2053. https://doi.org/10.1007/s00604-016-1846-z
[34] R. W. Raut, A. S. M. Haroon, Y. S. Malghe, B. T. Nikam, S. B. Kashid, Rapid biosynthesis of platinum and palladium metal nanoparticles using root extract of asparagus racemosus linn, *Advanced Materials Letters* **4** (2013) 650-654. https://doi.org/10.5185/amlett.2012.11470
[35] T. L. H. Nguyen, V.-D. Doan, Q.-H. Tran, A.T. Nguyen, A.V. Tran, V. T. Le, A. Renat Maratovich, H. Y. Hoang, Magnetic composite - Based dual nanozymes derived from coffee ground waste: A sustainable approach for colorimetric assay and prolonged reuse, *Microchemical Journal* **200** (2024) 110343. https://doi.org/10.1016/j.microc.2024.110343
[36] M. Cui, C. Wang, D. Yang, Q. Song, Fluorescent iridium nanoclusters for selective determination of chromium(VI), *Microchimica Acta* **185** (2018) 8. https://doi.org/10.1007/s00604-017-2553-0
[37] B. Wu, J. Yang, Y. Zu, J. Chi, K. Shi, Aligned electrospun fiber film loaded with multi - enzyme mimetic iridium nanozymes for wound healing, *Journal of Nanobiotechnology* **20** (2022) 478. https://doi.org/10.1186/s12951-022-01685-2
[38] M. Madej, D. Matoga, K. Skaźnik, R. Porada, B. Baś, J. Kochana, A voltammetric sensor based on mixed proton-electron conducting composite including metal-organic framework JUK-2 for determination of citalopram, *Microchimica Acta* **188** (2021) 184. https://doi.org/10.1007/s00604-021-04835-9
[39] A. Singh, P.K. Gautam, A. Verma, V. Singh, P. M. Shivapriya, S. Shivalkar, A. K. Sahoo, S. K. Samanta, Green synthesis of metallic nanoparticles as effective alternatives to treat antibiotics resistant bacterial infections, *Biotechnology Reports* **25** (2020) e00427. https://doi.org/10.1016/j.btre.2020.e00427
[40] Y. Peng, Q. Liu, B. Lu, T. He, F. Nichols, X. Hu, T. Huang, G. Huang, L. Guzman, Y. Ping, S. Chen, Organically Capped Iridium Nanoparticles as High-Performance Bifunctional Electrocatalysts for Full Water Splitting in Both Acidic and Alkaline Media: Impacts of Metal-Ligand Interfacial Interactions, *ACS Catalysis Journal* **11** (2021) 1179-1188. https://doi.org/10.1021/acscatal.0c03747
[41] J. Quinson, Iridium and IrOx nanoparticles: an overview and review of syntheses and applications, *Advances in Colloid and Interface Science* **303** (2022) 102643. https://doi.org/10.1016/j.cis.2022.102643
[42] A. E. F. Oliveira, C. Arnaldo, M. A. C. Resende, L. F. Ferreira, Gold Nanoparticles: A Didactic Step-by-Step of the Synthesis Using the Turkevich Method, Mechanisms, and Characterizations, *Analytica* **4** (2023) 250-263. https://doi.org/10.3390/analytica4020020
[43] Y. Yi, G. Weinberg, M. Prenzel, M. Greiner, S. Heumann, S. Becker, R. Schlögl, Electrochemical corrosion of a

glassy carbon electrode, *Catalysis Today* **295** (2017) 32-40. https://doi.org/10.1016/j.cattod.2017.07.013
[44] H. Keypour, S. G. Saremi, H. Veisi, M. Noroozi, Electrochemical determination of citalopram on new Schiff base functionalized magnetic Fe_3O_4 nanoparticle/MWCNTs modified glassy carbon electrode, *Journal of Electroanalytical Chemistry* **780** (2016) 160-168. https://doi.org/10.1016/j.jelechem.2016.08.022
[45] R. Piech, M. Rumin, B. Paczosa-Bator, High sensitive voltammetric determination of paroxetine on glassy carbon electrode modified with Nafion/MWCNTs, *International Journal of Electrochemical Science* **9** (2014) 7528-7539. https://doi.org/10.1016/S1452-3981(23)10985-0
[46] C. G. Sanz, S. H. P. Serrano, C. M. A. Brett, Electroanalysis of Cefadroxil Antibiotic at Carbon Nanotube/Gold Nanoparticle Modified Glassy Carbon Electrodes, *ChemElectroChem* **7** (2020) 2151-2158. https://doi.org/10.1002/celc.202000255
[47] H. Nouws, C. Delerue-Matos, A. Barros, Electrochemical determination of citalopram by adsorptive stripping voltammetry-determination in pharmaceutical products, *Analytical Letters* **39** (2006) 1907-1915. https://doi.org/10.1080/00032710600721712
[48] T. Madrakian, M. Soleimani, A. Afkhami, Electrochemical determination of fluvoxamine on mercury nanoparticle multi-walled carbon nanotube modified glassy carbon electrode, *Sensors and Actuators: B Chemical* **210** (2015) 259-266. https://doi.org/10.1016/j.snb.2014.12.074
[49] N. O. Gomes, C. D. Mendonça, S. A. S. Machado, O. N. Oliveira, P. A. Raymundo-Pereira, Flexible and integrated dual carbon sensor for multiplexed detection of nonylphenol and paroxetine in tap water samples, *Microchimica Acta* **188** (2021) 359. https://doi.org/10.1007/s00604-021-05024-4
[50] S. R. Al-Mhyawi, R. K. Ahmed, R. M. El Nashar, Application of a conducting poly-methionine/gold nanoparticles-modified sensor for the electrochemical detection of paroxetine, *Polymers (Basel)* **13** (2021) 3981. https://doi.org/10.3390/polym13223981
[51] R. F. Ajayi, E. Nxusani, S. F. Douman, A. Jonnas, P. G. L. Baker, E. I. Iwuoha, An amperometric cytochrome P450-2D6 biosensor system for the detection of the selective serotonin reuptake inhibitors (SSRIs) paroxetine and fluvoxamine, *Journal of Nano Research* **44** (2016) 208-228. https://doi.org/10.4028/www.scientific.net/JNanoR.44.208
[52] L. Daneshvar, G. H. Rounaghi, Z. Es'haghi, M. Chamsaz, S. Tarahomi, Fabrication a new modified electrochemical sensor based on Au-Pd bimetallic nanoparticle decorated graphene for citalopram determination, *Material Science and Engineering: C* **69** (2016) 653-660. https://doi.org/10.1016/j.msec.2016.07.025
[53] H. Ghaedi, A. Afkhami, T. Madrakian, F. Soltani-Felehgari, Construction of novel sensitive electrochemical sensor for electro-oxidation and determination of citalopram based on zinc oxide nanoparticles and multi-walled carbon nanotubes, *Material Science and Engineering: C* **59** (2016) 847-854. https://doi.org/10.1016/j.msec.2015.10.088